PCCP

Atomic force microscopic study on thermal and UV-irradiative formation and control of Au nano-particles on TiO_2(110) from $Au(PPh_3)(NO_3)$

Ken-ichi Fukui, Sho Sugiyama and Yasuhiro Iwasawa*

Department of Chemistry, Graduate School of Science, The University of Tokyo, Hongo, Bunkyo-ku, Tokyo, 113-0033, Japan. E-mail: iwasawa@chem.s.u.-tokyo.ac.jp; fax: +81-3-5800-6892

Received 10th April 2001, Accepted 27th June 2001
First published as an Advance Article on the web 6th August 2001

Formation of Au nano-particles on TiO_2(110) from a gold–phosphine complex $Au(PPh_3)(NO_3)$ was studied by environment-controlled atomic force microscopy (AFM). The Au complex began to agglomerate as particles larger than 4.2 nm in height on calcination in dry air at a temperature as low as 363 K. The size of the agglomerates reduced to 3.0 nm as a result of decomposition and combustion of the ligands by further calcination at 493 K for 4 h. UV irradiation of the Au-complex-deposited sample or of the TiO_2(110) substrate before deposition of the Au complex greatly reduced the size of the Au particles formed by the same calcination process to less than 1 nm, which falls in the range that has been claimed to show high catalytic activities for low-temperature CO oxidation. This may be a new preparation method that regulates the size of Au particles on flat oxide substrates.

1 Introduction

In recent years, it has been demonstrated that highly dispersed gold catalysts with inorganic oxide supports are tremendously active for low-temperature CO oxidation[1–14] and other reactions.[4,7,15,16] Low-temperature CO oxidation has been extensively studied as the key issue relevant to gas purification in the CO_2 laser, CO gas sensors, air-purification devices for respiratory protection, and pollution control devices for reducing industrial and environmental emission and removing trace CO from the ambient air in closed atmospheres such as submarines and space crafts on long duration missions.[1,4,17,18] Much work has also been devoted to exploitation of active oxygen species and the reaction mechanism for low-temperature CO oxidation on supported gold catalysts.[1,2,4,6,19–25] Supported gold catalysts showed an overall trend indicating that CO oxidation activity increased with decreasing size of the Au particles.[6,12] Recently, the relation between Au particle geometry and catalytic activity for CO oxidation has been studied by scanning tunneling microscopy/spectroscopy (STM/STS).[26,27]

We have developed a new preparation method to obtain highly active Au catalysts for low-temperature CO oxidation using an Au–phosphine complex $Au(PPh_3)(NO_3)$ as a precursor for Au particles and as-precipitated wet metal hydroxides [*e.g.* $Fe(OH)_3^*$, $Ti(OH)_4^*$] as precursors for metal oxide supports, followed by vacuum drying at room temperature and temperature-programmed calcination in air.[3,8–12] Some stages of the preparation procedure have been characterized by extended X-ray absorption fine structure (EXAFS), X-ray diffraction (XRD), ^{31}P solid state NMR, FT-IR, X-ray photoelectron spectroscopy (XPS), and transmission electron microscopy (TEM).[3,8–12] Use of the Au–phosphine complex was much more advantageous for catalyst preparation than that of the usual Au precursors like $HAuCl_4$, but it was still difficult to prepare highly active Au catalysts when conventional metal oxides such as Fe_2O_3 or TiO_2 were used as supports. These previous results motivated us to extend the work by using scanning probe microscopy (SPM), with particular interest in elucidating the behavior of Au–phosphine precursors and the factors that control the Au particle size on a TiO_2(110) single crystal as a typical flat oxide surface. Because of ease of handling the use of Au–phosphine complex as a precursor for the preparation of Au particles on a flat oxide substrate is more important than Au–metal vapor deposition in respect of industrial applications such as catalysts, gas sensors, *etc.*

The number of papers which deal with morphological changes of model oxide catalysts during preparation or during reaction is rather few.[28] Atomic force microscopy (AFM) is one of the methods suitable for such studies because many oxide substrates of chemical interest are insulators in their fully oxidized form after calcination. Several examples of AFM studies on the preparation procedures of model oxide catalysts are CuO_x on SiO_2 prepared by a spin coating method,[29–31] the growth of Pt–Rh alloy crystallites on α-Al_2O_3 by thermal treatment,[32] and the preparation of an Ag/α-Al_2O_3 catalyst from an aqueous precursor ($AgNO_3$).[33] Morphological changes of Pd/SiO_2 thin film catalysts during 1,3-butadiene hydrogenation,[34] changes in morphology of MoO_3 during reduction with H_2,[35] or alcohols,[36–38] creation of active sites for selective oxidation of isobutylene during the reaction on MoO_3 mixed with α-Sb_2O_4,[39] and breakup of CrO_x/SiO_2 catalyst particles during ethylene polymerization[40] have all been characterized by means of AFM.

In the present paper, the formation of Au nano-particles on TiO_2(110) from a gold–phosphine complex $Au(PPh_3)(NO_3)$ was studied by AFM. It was found that the Au precursor agglomerated to large particles by calcination in dry air at temperatures as low as 363 K. The average height of Au particles formed by calcination at 493 K for 4 h was 3.0 nm, which cannot be expected to show high catalytic activities.[6,12,26] UV irradiation to the sample prior to calcination greatly reduced the size of the Au particles to less than 1 nm,

whose size is reported to have high catalytic activities.[6,12,26] This may be a new preparation method that regulates the size of Au particles, which is relevant to catalytic activities.

2 Experimental

The experiments were performed in an environment-controlled AFM chamber based on a commercial SPM system (JEOL JSTM4200). The AFM chamber is evacuated by a turbomolecular pump, or by a rotary pump and gases in the pressure range 5×10^{-4} Pa to *ca.* 1 atm (1.0×10^5 Pa) can be introduced into the chamber in a controlled manner. A TiO_2(110) sample was mounted on a pyrolytic boron nitride/pyrolytic graphite heater and the sample temperature during heating was estimated by a separate experiment where the temperature was monitored by a K-type thermocouple attached to the sample. The sample can be transferred between the AFM chamber and a glove box without exposing it to air using a small transfer container that can be purged with inert gas. Therefore, AFM observation of surfaces after deposition of air-sensitive chemicals is possible.

The gold complex $Au(PPh_3)(NO_3)$ was synthesized according to the literature.[41] A polished TiO_2(110) wafer of $9.5 \times 2 \times 0.25$ mm^3 (Earth Chemical) was calcined in air at 1073 K for 1 h before use. The sample was flashed at 800 K in the SPM chamber under high vacuum less than 10^{-3} Pa. After observation of the surface structure by AFM, the sample was packed in the transfer container and purged with N_2 gas (99.99%). The container was opened in the glove box purged with N_2 gas (99.99%) and 0.2 μl of acetone (Aldrich HPLC grade) solution of $Au(PPh_3)(NO_3)$ (10 wt.%) was dropped on the sample surface in the glove box. The solution covered at least 3 mm^2 and the solvent quickly became invisible by evaporation. The deposited sample was packed in the container filled with N_2 gas and transferred to the AFM chamber at high vacuum. The deposited sample was exposed to visible light as little as possible because $Au(PPh_3)(NO_3)$ is light-sensitive.[41] The sample was calcined in the AFM chamber under a flow of dry air (1 atm) at a heating rate of *ca.* 30 K min^{-1} to temperatures of 313, 363, 423 and 493 K, held for 30 min, and cooled to RT. Finally, the sample was calcined at 493 K for 3.5 h (4 h in total). After each calcination, surface structures were observed by AFM.

AFM measurements were performed under high vacuum ($< 5 \times 10^{-4}$ Pa) at RT operated in a non-contact mode. Non-contact mode uses a negative shift of the resonance frequency of the cantilever as a feedback signal to control the Z piezo. Therefore, the tip–sample distance is regulated by the relatively long-range attractive force between the tip and the sample. Atomic scale structures of a TiO_2(110) surface including oxygen point defects[42–44] and adsorbed molecules on them[45–47] were successfully visualized using this mode due to its small interaction for imaging. For the AFM measurements, stiff silicon cantilevers (Olympus) with a resonance frequency of ~300 kHz and a force constant of ~20 N m^{-1} were used as the force sensor. The oscillation amplitude of the cantilever was set at ~30 $nm_{p\text{-}p}$ and the frequency shift was set at ~45 Hz. Surface structures were recorded as frequency shift (constant height) images and topographic (constant frequency shift) images.

Most of the images shown in the present paper are frequency shift images because better spatial resolution was achieved with such images. Detection of frequency shift during constant height scanning was relatively easy and it took 183 s per frame for a 500×500 nm^2 scan. On the other hand, a slower scan was needed for topography measurements to regulate frequency shift and it took 732 s per frame for the same area. Unfortunately, the feedback electronics of our apparatus is not stable enough to obtain topographic images of 500×500 nm^2 area at a quality as high as frequency shift images. Note that we can measure the height of the particles reasonably along the fast scan (horizontal) direction (it takes 1.4 s per line). Thus, the height of Au particles formed on the surface was measured in topographic images of the corresponding area.

UV light irradiation was performed using a 100 W Hg lamp through a Pyrex glass bell jar of the AFM chamber. UV light between 300 and 550 nm was selected and focused on the sample through a lens system including a dichroic mirror. The rise in the sample temperature during irradiation for 5 h was less than 60 K.

Decomposition and desorption of the ligands of the Au complex were analyzed by a thermogravimetric (TG) analyzer (Rigaku TG8120). For the analysis, rutile TiO_2 powder (2.91 m^2 g^{-1}) was impregnated with an acetone (Aldrich HPLC grade) solution of $Au(PPh_3)(NO_3)$ under vigorous stirring for 1 h, followed by evacuation at room temperature for 2 h to remove the solvent. The loading of $Au(PPh_3)(NO_3)$ on the support was controlled to be 9.8 wt.%. The calculated amount of Au per unit surface area is similar to that used for AFM measurements. The sample was heated from RT to 493 K at a constant rate of 5 K min^{-1} and held at 493 K for 4 h.

3 Results

3.1 Formation of Au particles by calcination of an as-deposited $Au(PPh_3)(NO_3)/TiO_2$(110) sample

Fig. 1 shows an AFM image of a calcined TiO_2(110) surface. The surface was flat with a root mean square (RMS) height value of 0.31 nm. Monatomic steps (0.33 nm per step) were observed near the edge of the sample probably due to small misalignment during polishing of the sample. An AFM image after deposition of $Au(PPh_3)(NO_3)$ on the TiO_2(110) surface is shown in Fig. 2(a). Although $Au(PPh_3)(NO_3)$ should have covered the surface if we consider the amount deposited, no significant difference in surface morphology was observed before and after the deposition. Figs. 2(b)–(f) show AFM images after calcination of the sample of Fig. 2(a) at given temperatures. Large particles were formed on the surface after calcination at 363 K [Fig. 2(c)], but they changed to smaller particles after calcination at 493 K [Figs. 2(e) and (f)]. Fig. 3 summarizes the data obtained at each calcination temperature as histograms. The height of each particle was determined directly from the topographic images.

It is well known that the shape of the particles of nanometre size obtained by AFM is greatly modified because the apex of the probe tip has comparable size.[29,48] It is schematically shown in Fig. 4(a) how the tip traces a nanometre-scale particle. Here we simply assume that the tip traces the substrate structure, keeping the minimum vertical component of the dis-

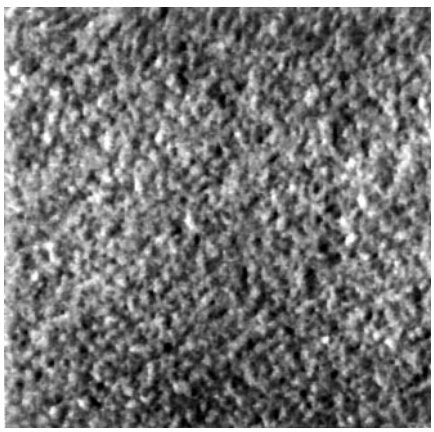

Fig. 1 AFM image (500×500 nm^2) of a TiO_2(110) surface after calcination at 1073 K in air for 1 h.

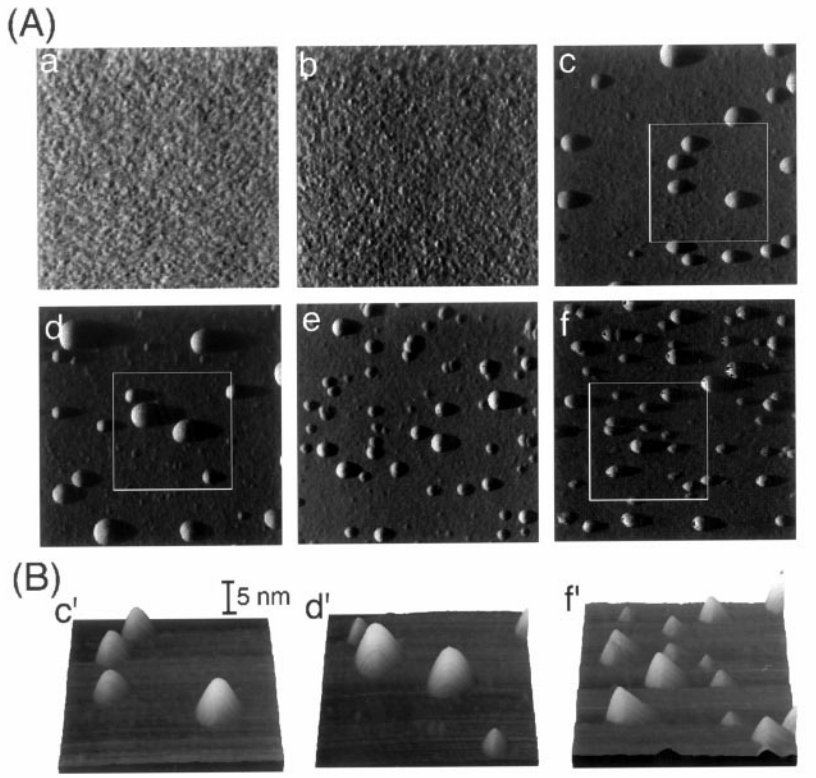

Fig. 2 AFM images (500 × 500 nm^2) at different stages of calcination of (a) an Au(PPh$_3$)(NO$_3$)-deposited TiO$_2$(110) surface. Each image was obtained at RT after calcination of (a) in the AFM chamber under 1 atm of dry air at (b) 313 K for 30 min, (c) 363 K for 30 min, (d) 423 K for 30 min, (e) 493 K for 30 min and (f) 493 K for 4 h, respectively. (A) Frequency shift images. (B) Topographic images of the square areas of (c), (d) and (f) in (A).

tance between the tip and the sample constant. Only the vertical component of the attractive force determined by the distance between the atoms of the tip and the sample gives effects on the frequency shift because, in the non-contact mode, the cantilever vibrates in a direction almost perpendicular to the surface and only the deflection in the plane of vibration is detected. To obtain a more precise picture, integration of the attractive forces between each atom of the tip and the

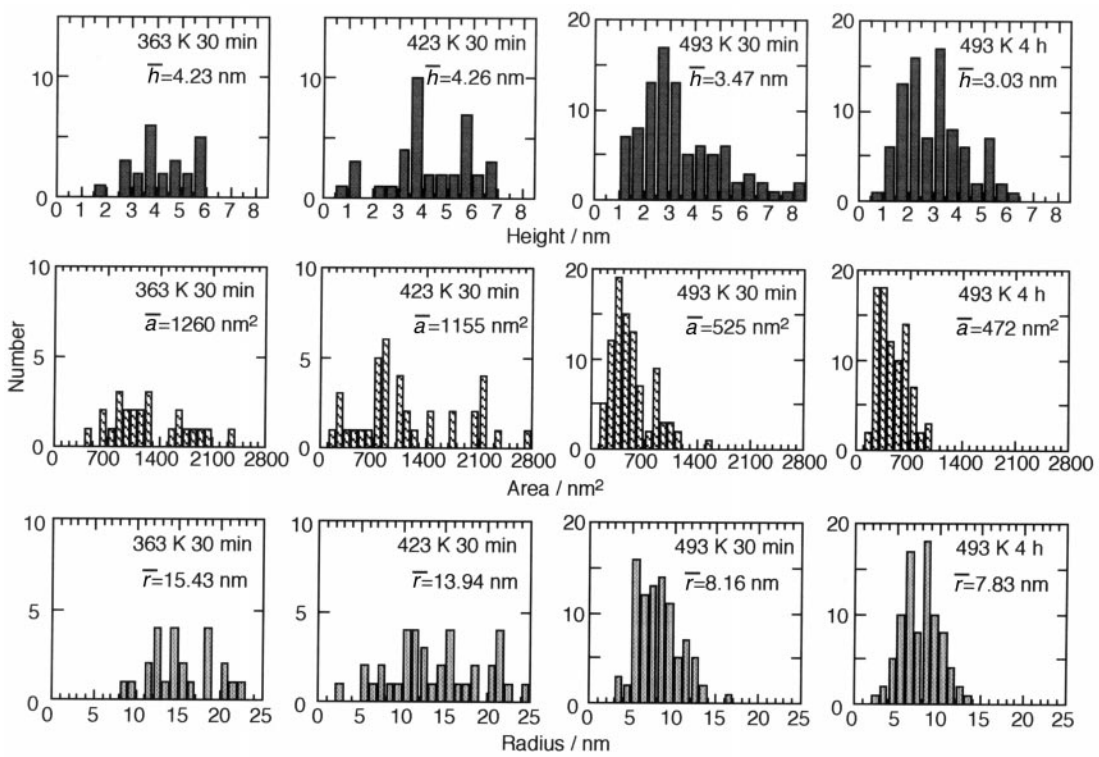

Fig. 3 Histograms of the particles in height (top), area (middle) and radius (bottom), which were observed by AFM after calcination of an Au(PPh$_3$)(NO$_3$)-deposited TiO$_2$(110) surface at 363 K for 30 min (first column), 423 K for 30 min (second column), 493 K for 30 min (third column) and 493 K for 4 h (fourth column), respectively. The data from six separate regions of 250 × 250 nm^2 were summed up. The height and area were derived from the apparent height of the particles and their projected shape onto the surface, respectively. The radius was derived after shape deconvolution of the tip and the particle. See details in the text. Average values ($\bar{h}$, $\bar{a}$ and $\bar{r}$) are shown in each histogram.

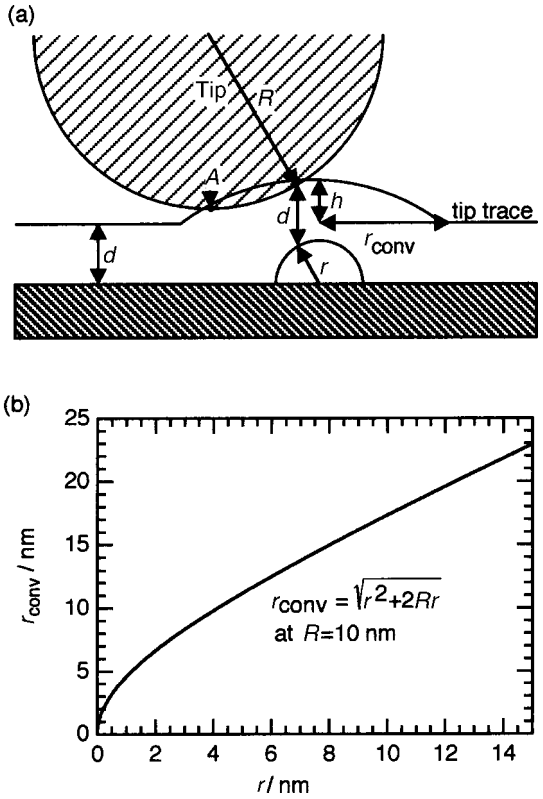

Fig. 4 (a) Schematic model of the trace of the AFM tip at an adparticle measured in the non-contact mode. It assumes that the tip traces the substrate structure, keeping the minimum vertical component of the distance between the tip and the sample (d) constant. The shapes of the tip and the adparticle are assumed to be hemispheres with radius of R and r ($r = h$), respectively. The trace of the tip apex (A) is drawn as a solid line. The shape convolution of the tip and the particle results in expansion in the observed size of the particle along the surface ($r_{conv} > r$). (b) Simulated r_{conv} as a function of r. The radius of the tip apex R is assumed to be 10 nm, which is a typical value for the cantilevers used in the present study.

sample considering a force–distance curve for each case is necessary. However, Fig. 4(a) can qualitatively explain the phenomenon; the tip traces the particle as a much wider one. Note that the height (h) of the particle imaged by AFM is unchanged under this assumption. Fig. 4(b) shows a simulation curve of the convoluted radii. By assuming that each particle observed by AFM in Fig. 2 is a hemi-oval and the radius (R) of the tip apex is 10 nm, the apparent radius was calculated by deconvolution and summarized as histograms at the bottom in Fig. 3. Note that the calculated radius greatly depends on the assumptions made and it is not appropriate to discuss the shape of the particles in detail from the AFM images. Fig. 3 shows that the Au particles on $TiO_2(110)$ from $Au(PPh_3)(NO_3)$ readily grow to large ones which cannot be expected to have a high activity for low-temperature CO oxidation.[6,12]

3.2 Effect of UV irradiation of the as-deposited $Au(PPh_3)(NO_3)/TiO_2(110)$ sample on the growth of Au particles

UV irradiation of the as-deposited $Au(PPh_3)(NO_3)/TiO_2(110)$ sample was examined. The Au complex was reported to be light-sensitive.[41] If the complex is first decomposed on the surface by UV irradiation, suppression of surface migration of the precursor may reduce the particle size. The reduction in particle size is obvious in Fig. 5, which is a series of AFM images after calcination at given temperatures following UV irradiation. It seems that small particle species increased by UV irradiation [Fig. 5(a)], but the size is negligible compared with those formed by subsequent calcination [Figs. 5(b)–5(f)]. Actually, the RMS value of topography in Fig. 5(a) was 0.35 nm which is almost the same as that of Fig. 2(b). The distribution of the particle heights after calcination is shown in Fig. 6. The average height of the particle was less than 1 nm and the density of the particles was higher than in Fig. 2 in accordance with reduction in the particle size. The particles consist of two to six layers of Au with its center at three layers judging from

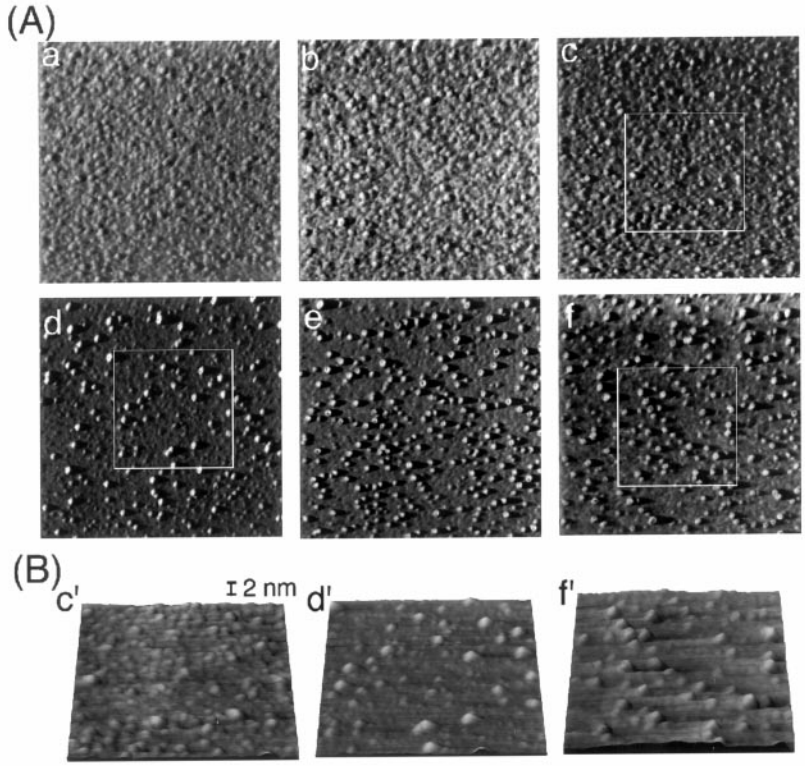

Fig. 5 AFM images (500 × 500 nm^2) at different stages of calcination of an $Au(PPh_3)(NO_3)$-deposited $TiO_2(110)$ surface after UV irradiation of the sample for 5 h. Each image was obtained at RT after calcination of (a) in the AFM chamber under 1 atm of dry air at (b) 313 K for 30 min, (c) 363 K for 30 min, (d) 423 K for 30 min, (e) 493 K for 30 min and (f) 493 K for 4 h, respectively. (A) Frequency shift images. (B) Topographic images of the square areas of (c), (d) and (f) in (A).

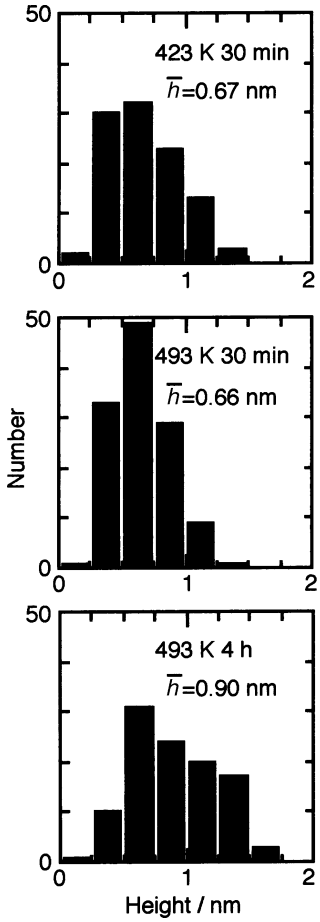

Fig. 6 Histograms of the particle heights, which were observed by AFM after calcination of an $Au(PPh_3)(NO_3)$-deposited and UV-irradiated $TiO_2(110)$ surface at 423 K for 30 min, 493 K for 30 min and 493 K for 4 h, respectively. The data from three separate regions of 250 × 250 nm^2 were summed up. The average height ($\bar{h}$) is shown in each histogram.

the height. This falls in the range which is claimed to show a high catalytic activity for CO oxidation by combination with STM measurements.[26] Further calcination of the sample at 673 K in a glove box under 1 atm of dry air did not change the morphology of the Au particles.

3.3 Effect of UV irradiation of the $TiO_2(110)$ substrate prior to deposition of $Au(PPh_3)(NO_3)$ on the growth of Au particles

Part of the UV light used in this study (300–550 nm) has a larger energy than the bandgap of rutile TiO_2 (*ca.* 3.2 eV). Thus, it can form electron–hole pairs by transition of electrons from the valence band to the conduction band. A $TiO_2(110)$ substrate in the AFM chamber (1×10^{-4} Pa) was irradiated with UV for 5 h prior to deposition of the Au complex precursor. Fig. 7(a) shows an AFM image of a UV-irradiated $TiO_2(110)$ surface. No significant change in surface topography was observed. Fig. 7(b) and 7(c) show AFM images after deposition of $Au(PPh_3)(NO_3)$ on the UV-irradiated surface and after subsequent calcination of the sample at 493 K for 4 h, respectively. The size of Au particles in Fig. 7(c) was much smaller than that without UV irradiation [Fig. 2(f)] and similar to that in Fig. 5(f). This suggests that the major reason for the reduction in the Au particle size is some change in the nature of the TiO_2 substrate. This will be discussed later.

3.4 Decomposition process of $Au(PPh_3)(NO_3)$ on TiO_2

To obtain some insights into the decomposition process of $Au(PPh_3)(NO_3)$ on TiO_2, thermogravimetric analysis (TGA) was performed. Rutile-type TiO_2 crystalline powder was used as a substrate because the surface area of a single crystal is too small for TGA. Table 1 summarizes the loss in weight of the sample during calcination in air. It indicates that little change happens up to 423 K. Two steps of loss in weight were observed in the TGA curve; one was observed between 423 and 473 K during heating at a rate of 5 K min^{-1} and the other was observed during the first 1 h keeping the temperature at 493 K. In the former change, weight loss was *ca.* 7%. Differential thermal analysis (DTA) performed simultaneously with TGA indicated that an endothermic process began at *ca.* 423 K and that it changed to an exothermic process at *ca.* 473 K. In our previous paper,[3] we showed by FT-IR that $Au(PPh_3)(NO_3)$ dissociated to form $[Au(PPh_3)]^+$ and NO_3^- species on a Ti oxide substrate at RT, and this NO_3^- species disappeared by calcination at 473 K.[49] NO_3 has 11.9% of total weight of the complex. Thus, desorption of NO_3 ligands as NO_2 probably begins at *ca.* 423 K. Oxidative decomposition of PPh_3 ligands may be responsible for the following exothermic process. In the latter weight loss process, combustion and/or desorption of detached ligands may occur. Preliminary X-ray diffraction measurement of this sample showed that diffraction of Au(111) and Au(200) appeared after this calcination procedure. Formation of metallic gold particles by this calcination procedure is also supported by our

Table 1 Thermogravimetric analysis (TGA) of an $Au(PPh_3)(NO_3)/TiO_2$ (powder) sample (9.8 wt.%). The sample was heated from RT to 493 K at a rate of 5 K min^{-1} and held for 4 h at 493 K. Cumulative loss in weight is expressed in per cent by calculation which assumes that all the loss in sample weight came from the $Au(PPh_3)(NO_3)$ complex

T/K	Cumulative loss in weight (%)
313	0.4
363	1.8
423	3.3
493 (0 min)	10.0
493 (30 min)	33.9
493 (4 h)	40.1

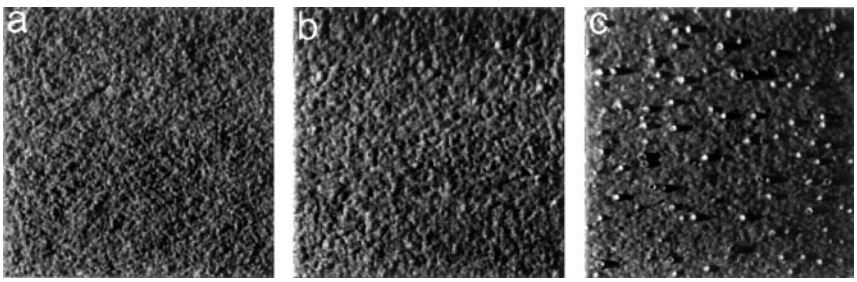

Fig. 7 AFM images (500 × 500 nm^2) of (a) a $TiO_2(110)$ surface after UV irradiation for 5 h, (b) the surface after deposition of $Au(PPh_3)(NO_3)$ on (a) and (c) the surface after calcination of (b) in the AFM chamber under 1 atm of dry air at 493 K for 4 h. The calcination procedure was the same as that in Figs. 2 and 5, but only the AFM image of the finally treated surface is shown here in (c).

previous X-ray photoelectron spectroscopy (XPS) measurements on another TiO_2 substrate (Degussa, P25).[10] If we assume that only metallic Au and P_2O_5 were left on the surface by calcination, the weight loss is calculated to be 48.6%.

4 Discussion

4.1 Agglomeration of the Au complex on a TiO_2 single crystal surface at low temperature

Annealing of $Au(PPh_3)(NO_3)$ deposited on $TiO_2(110)$ at 363 K in a dark environment led to the formation of large particles [Fig. 2(c)]. The results of TGA indicated that no desorption of the ligands from the deposited Au complex occurred at 363 K. Therefore, the large particles in Fig. 2(c) are agglomerates of the Au complex $Au(PPh_3)(NO_3)$. The deposited Au complexes do not migrate enough to make large particles at 313 K as shown in Fig. 2(b). Further agglomeration of $Au(PPh_3)(NO_3)$ to large particles occurred by calcination at 423 K for 30 min [Fig. 2(d)].

The previous FT-IR, EXAFS, ^{31}P CP/MAS-NMR and XRD measurements demonstrated that the Au–phosphine complex deposited on TiO_2 (Degussa, P25) began to decompose partly to metallic Au particles by calcination at 473 K.[3,9,10] These results are consistent with the AFM image in Fig. 2(e), where the size of the particles reduced in accordance with the increase in the density by calcination at 493 K for 30 min, suggesting that some particles were divided into pieces and, at the same time, detachment and, combustion of the ligands of the Au complexes on $TiO_2(110)$ occurred as indicated by TGA and DTA. The exothermic process of the combustion of the agglomerated particles in Fig. 2(d) may be a driving force for the redispersion of the particles in Fig. 2(e). The dispersed particles in Fig. 2(e) consist of Au crystallites as proved by XRD. The 4 h calcination at 493 K did not increase the Au particle size as shown in Fig. 3.

4.2 Effect of UV irradiation on the reduction of Au particle size on the TiO_2 single crystal surface

UV irradiation of an Au complex-deposited TiO_2 sample and UV irradiation of the TiO_2 substrate itself before deposition of the Au complex remarkably reduced the size of Au particles formed by the following calcination. These facts suggest that the major reason for the reduction in particle size is some change in the nature of the TiO_2 substrate.

It has been reported that amphiphilicity was changed by UV irradiation of TiO_2 surfaces.[50] A TiO_2 surface is hydrophobic before UV irradiation, showing a high water contact angle. However, UV irradiation to the substrate in air dramatically decreases the contact angle to nearly zero, resulting in the spreading out of a water droplet on the surface. The phenomenon was supposed to be due to the formation of hydroxy groups on TiO_2 as follows.[50] Irradiation by UV light that has higher energy than the bandgap of TiO_2 creates electron–hole pairs. Some of the holes decrease the oxygen anion, forming an oxygen vacancy. In the presence of water, water molecules preferentially dissociate at the vacancy, forming hydroxy groups.

If we consider the base pressure of our AFM chamber of *ca.* 5×10^{-4} Pa without baking, the TiO_2 surface may be covered with a water layer. Then surface hydroxy groups may be formed on the surface by UV irradiation. Comparing Fig. 5 to Fig. 2, and also comparing the average particle height in Fig. 6 with that in Fig. 3, suppression of the agglomeration of the $Au(PPh_3)(NO_3)$ precursor at low temperatures seems to be a key issue to obtain small Au metallic particles. Concentration of hydroxy groups of oxide surfaces may be regarded as an important issue to obtain small metal particles.[3,12,51] Indeed, we have shown[3] that reaction and interaction between $Au(PPh_3)(NO_3)$ and surface hydroxy groups of oxide supports is a reason for the formation of smaller Au particles on TiO_2.

Partial decomposition or detachment of the PPh_3 ligand may occur during UV irradiation to the $Au(PPh_3)(NO_3)$-deposited $TiO_2(110)$ surface, because $Au(PPh_3)(NO_3)$ is light-sensitive.[41] Partial decomposition may also prevent the $Au(PPh_3)(NO_3)$ precursor from forming agglomerates at low calcination temperatures due to reduction of the mobility as we supposed. Au particles less than 10 nm were formed on TiO_2 by photoreduction of $AuCl_4^-$ in an $HAuCl_4$ solution containing colloidal TiO_2.[52] The Au–phosphine complex seems to be more controllable to prepare smaller Au metallic particles on TiO_2. It has also been reported that UV irradiation of a TiO_2 substrate decreases the contact angle of oily liquids as well as water.[50] The change in the nature of the TiO_2 surface may disperse $Au(PPh_3)(NO_3)$ more on the UV-irradiated surface, which may also suppress agglomeration during calcination. However, these factors are not major because similar sizes of Au particles were obtained between the two samples UV irradiated before and after deposition of the Au complex [Figs. 7(c) and 5(f)].

5 Summary

Formation and control of Au nano-particles on $TiO_2(110)$ from a gold–phosphine complex $Au(PPh_3)(NO_3)$ were observed by an environment-controlled AFM. AFM images and TGA experiments indicated that the Au–phosphine precursors agglomerated as large particles of 4.3 nm in height by calcination in dry air at 363 K. This is probably due to migration of the Au precursor on $TiO_2(110)$ and small interaction between the Au precursor and the TiO_2 substrate. The size of the agglomerates reduced to 3.0 nm high as a result of decomposition and combustion of the ligands by calcination at 493 K for 4 h. However, this size cannot be expected to show high catalytic activities for low-temperature CO oxidation. UV irradiation to an Au-complex-deposited TiO_2 sample prior to calcination remarkably reduced the size of the produced Au particles to less than 1 nm. UV irradiation of the $TiO_2(110)$ substrate before deposition of the Au-phosphine complex also decreased the size of the produced Au particles to less than 1 nm. The phenomenon may be due to the formation of hydroxy groups on the TiO_2 surface by UV irradiation. Surface hydroxy groups probably promote the interaction with the Au precursors and prevent the precursors from agglomerating at low calcination temperatures. UV irradiation may be a new preparation method that regulates the size of Au particles on flat oxide substrates.

Acknowledgements

This work has been supported by CREST (Core Research for Evolutional Science and Technology) of Japan Science and Technology Corporation (JST).

References

1 G. C. Bond and D. T. Thompson, *Catal. Rev. Sci. Eng.*, 1999, **41**, 319.
2 G. C. Bond and D. T. Thompson, *Gold Bull.*, 2000, **33**, 41.
3 A. I. Kozlov, A. P. Kozlova, H. Liu and Y. Iwasawa, *Appl. Catal. A*, 1999, **182**, 9.
4 M. Haruta, *Catal. Surv. Jpn.*, 1997, **1**, 61.
5 M. Haruta, N. Yamada, T. Kobayashi and S. Iijima, *J. Catal.*, 1989, **115**, 301.
6 M. Haruta, S. Tsubota, T. Kobayashi, H. Kageyama, M. J. Genet and B. Delmon, *J. Catal.*, 1993, **144**, 175.
7 M. Haruta, A. Ueda, S. Tsubota and R. M. Torres-Sanchez, *Catal. Today*, 1996, **29**, 443.
8 Y. Yuan, K. Asakura, H. Wan, K. Tsai and Y. Iwasawa, *Chem. Lett.*, 1996, 755.

9 Y. Yuan, A. P. Kozlova, K. Asakura, H. Wan, K. Tsai and Y. Iwasawa, *J. Catal.*, 1997, **170**, 191.
10 Y. Yuan, K. Asakura, A. P. Kozlova, H. Wan, K. Tsai and Y. Iwasawa, *Catal. Today*, 1998, **44**, 333.
11 A. P. Kozlova, S. Sugiyama, A. I. Kozlov, K. Asakura and Y. Iwasawa, *J. Catal.*, 1998, **176**, 426.
12 A. I. Kozlov, A. P. Kozlova, K. Asakura, Y. Matsui, T. Kogure, T. Shido and Y. Iwasawa, *J. Catal.*, 2000, **196**, 56.
13 A. M. Visco, A. Donato, C. Milone and S. Galvagno, *React. Kinet. Catal. Lett.*, 1997, **61**, 219.
14 T. J. Mathieson, A. G. Langdon, N. B. Milestone and B. K. Nicholson, *J. Chem. Soc., Chem. Commun.*, 1998, 371.
15 H. Sakurai and M. Haruta, *Appl. Catal. A*, 1995, **127**, 93.
16 D. Andreeva, V. Idakiev, T. Tabakova and A. Andreev, *J. Catal.*, 1996, **158**, 354.
17 G. B. Hoflund, S. D. Gardner, D. R. Schryer, B. T. Upchurch and E. J. Kielin, *Appl. Catal. B*, 1995, **6**, 117.
18 G. J. Hutchings, M. R. H. Siddigui, A. Burrows, C. J. Kiely and R. Whyman, *J. Chem. Soc., Faraday Trans.*, 1997, **93**, 187.
19 F. Boccuzzi, A. Chiorino, S. Tsubota and M. Haruta, *J. Phys. Chem.*, 1996, **100**, 3625.
20 A. Knell, P. Barnickel, A. Baiker and A. Wokaun, *J. Catal.*, 1992, **137**, 306.
21 S. D. Lin, M. Bollinger and M. A. Vannice, *Catal Lett.*, 1993, **17**, 245.
22 H. Liu, A. I. Kozlov, A. P. Kozlova, T. Shido, K. Asakura and Y. Iwasawa, *J. Catal.*, 1999, **185**, 252.
23 H. Liu, A. I. Kozlov, A. P. Kozlova, T. Shido and Y. Iwasawa, *Phys. Chem. Chem. Phys.*, 1999, **1**, 2851.
24 M. Olea, M. Kunitake, T. Shido, K. Asakura and Y. Iwasawa, *Bull. Chem. Soc. Jpn.*, 2001, **74**, 255.
25 M. Olea, M. Kunitake, T. Shido and Y. Iwasawa, *Phys. Chem. Chem. Phys.*, 2001, **3**, 627.
26 M. Valden, X. Lai and D. W. Goodman, *Science*, 1998, **281**, 1647.
27 M. Valden, S. Pak, X. Lai and D. W. Goodman, *Catal. Lett.*, 1998, **56**, 7.
28 E. M. Gaigneaux, *Curr. Opin. Solid State Mater. Sci.*, 1998, **3**, 343.
29 A. Partridge, S. L. G. Toussaint, C. F. J. Flipse, L. J. van Ijzendoorn and L. C. A. van den Oetelaar, *J. Vac. Sci. Technol. B*, 1996, **14**, 585.
30 L. C. A. van den Oetelaar, A. Partridge, P. J. A. Stapel, C. F. J. Flipse and H. H. Brongersma, *J. Phys. Chem. B*, 1998, **102**, 9532.
31 M. A. Brookshier, C. C. Chusuei and D. W. Goodman, *Langmuir*, 1999, **15**, 2043.
32 K. Okumura, S. Hyodo, S. Noda and Y. Maruyama, *J. Phys. Chem. B*, 1998, **102**, 2350.
33 D. P. C. Bird, C. M. C. de Castilho and R. M. Lambert, *Surf. Sci.*, 2000, **449**, L221.
34 K. H. Lee and E. E. Wolf, *Catal. Lett.*, 1994, **26**, 297.
35 R. L. Smith and G. S. Rohrer, *J. Catal.*, 1996, **163**, 12.
36 R. L. Smith and G. S. Rohrer, *J. Catal.*, 1998, **173**, 219.
37 R. L. Smith and G. S. Rohrer, *J. Catal.*, 1998, **180**, 270.
38 R. L. Smith and G. S. Rohrer, *J. Catal.*, 1999, **184**, 49.
39 E. M. Gaigneaux, P. Ruiz, E. E. Wolf and B. Delmon, *Appl. Surf. Sci.*, 1997, **121**, /122, 552.
40 V. J. Ruddick and J. P. S. Badyal, *J. Phys. Chem. B*, 1997, **101**, 1791.
41 A. M. Mueting, B. D. Alexander, P. D. Boyle, A. L. Casalnuovo, L. N. Ito, B. J. Johnson and L. H. Pignolet, in *Inorganic Synthesis*, Vol. 29, ed. R. N. Grimes, Wiley, New York, 1992, p. 280.
42 K. Fukui, H. Onishi and Y. Iwasawa, *Phys. Rev. Lett.*, 1997, **79**, 4202.
43 Y. Iwasawa, *Surf. Sci.*, 1998, **402**, 404, 8.
44 Y. Iwasawa, H. Onishi, K. Fukui, S. Suzuki and T. Sasaki, *Faraday Discuss.*, 1999, **114**, 259.
45 K. Fukui, H. Onishi and Y. Iwasawa, *Chem. Phys. Lett.*, 1997, **280**, 296.
46 K. Fukui, H. Onishi and Y. Iwasawa, *Appl. Surf. Sci.*, 1999, **140**, 259.
47 K. Fukui and Y. Iwasawa, *Surf. Sci.*, 2000, **464**, L719.
48 K. Fukui and Y. Iwasawa, *Surf. Sci.*, 1999, **441**, 529.
49 S. Sugiyama, K. Fukui and Y. Iwasawa, unpublished data.
50 R. Wang, K. Hashimoto, A. Fujishima, M. Chikuni, E. Kojima, A. Kitamura, M. Shimohigoshi and T. Watanabe, *Nature*, 1997, **388**, 431.
51 J. A. Schwarz, C. Contescu and A. Contescu, *Chem. Rev.*, 1995, **95**, 477.
52 C. Y. Wang, C. P. Liu, J. Chen and T. Shen, *J. Colloid Interface Sci.*, 1997, **191**, 464.